Physics

Physics Research Publications

Purdue University *Year* 2011

Spin Waves in the (pi, 0) Magnetically Ordered Iron Chalcogenide Fe1.05Te

O. J. Lipscombe, G. F. Chen, C. Fang, T. G. Perring, D. L. Abernathy, A. D. Christianson, T. Egami, N. L. Wang, J. P. Hu, and P. C. Dai

Spin Waves in the $(\pi, 0)$ Magnetically Ordered Iron Chalcogenide $Fe_{1.05}Te$

O. J. Lipscombe,[1] G. F. Chen,[2] Chen Fang,[3] T. G. Perring,[4,5] D. L. Abernathy,[6] A. D. Christianson,[6] Takeshi Egami,[1,6] Nanlin Wang,[2] Jiangping Hu,[3,2] and Pengcheng Dai[1,6,2,*]

[1]*The University of Tennessee, Knoxville, Tennessee 37996-1200, USA*
[2]*Institute of Physics, Chinese Academy of Sciences, Beijing 100080, China*
[3]*Department of Physics, Purdue University, West Lafayette, Indiana 47907, USA*
[4]*ISIS Facility, STFC Rutherford Appleton Laboratory, Didcot, Oxfordshire OX11 0QX, United Kingdom*
[5]*Department of Physics and Astronomy, University College London, London WC1E 6BT, United Kingdom*
[6]*Oak Ridge National Laboratory, Oak Ridge, Tennessee 37831, USA*

(Received 11 November 2010; published 4 February 2011)

We use neutron scattering to show that spin waves in the iron chalcogenide $Fe_{1.05}Te$ display novel dispersion clearly different from both the first principles density functional calculations and recent observations in the related iron pnictide $CaFe_2As_2$. By fitting to a Heisenberg Hamiltonian, we find that although the nearest-neighbor exchange couplings in the two systems are quite different, their next-nearest-neighbor (NNN) couplings are similar. This suggests that superconductivity in the pnictides and chalcogenides share a common magnetic origin that is intimately associated with the NNN magnetic coupling between the irons.

DOI: 10.1103/PhysRevLett.106.057004 PACS numbers: 74.70.Xa, 75.30.Ds, 78.70.Nx

All parent compounds of cuprate superconductors are antiferromagnetic (AFM) Mott insulators characterized by the same local moment Heisenberg Hamiltonian [1]. For this reason, it is believed that magnetism is important for the high-T_c superconductivity [2]. The iron-based superconductors [3,4] share many features in common with the cuprates, which leads many to conjecture that the magnetism present in these compounds is vital for the presence of superconductivity. The iron-based superconductors can be divided into two chemical classes, the iron pnictides such as $CaFe_2As_2$ and iron chalcogenides $Fe_{1+y}Te$. Many properties of the pnictides and chalcogenides are similar, including similar band structure [5] and magnetic excitations in the superconducting compositions [6–12]. Furthermore, the magnetism in the pnictide parent $CaFe_2As_2$ [Fig. 1(b)] is consistent with first principles density functional calculations [13]. However, the parent compound [14,15] of the iron chalcogenides, $Fe_{1+y}Te$, possesses a different AFM order [Fig. 1(a)]. Therefore, it is important to determine if magnetism in these two systems can be described by a similar Hamiltonian. If the magnetic description between systems is entirely dissimilar, then it presents a serious challenge to many theories [16–19] where superconductivity has a magnetic origin.

By studying the spin waves in $Fe_{1.05}Te$, we compare the magnetic couplings within the pnictide and chalcogenide systems. We show that although the nearest-neighbor (NN) couplings in the two systems are very different, the effective next-nearest-neighbor couplings (NNN) J_2 are very similar. While our results are consistent with the theoretical idea that J_2 is important for superconductivity [18], the isotropic J_2 we find in $Fe_{1.05}Te$ is very different from the anisotropic J_2 yielded from density functional calculations [20]. Our results suggest that while the NN coupling may change, it is the NNN coupling that persists between different iron superconductors.

We have used time-of-flight inelastic neutron spectroscopy to determine the dispersion of spin-wave excitations in $Fe_{1.05}Te$ (with AFM ordering temperature $T_N = 68$ K; see Fig. 1(d) and Ref. [21]), the $x = 0$ (nonsuperconducting)

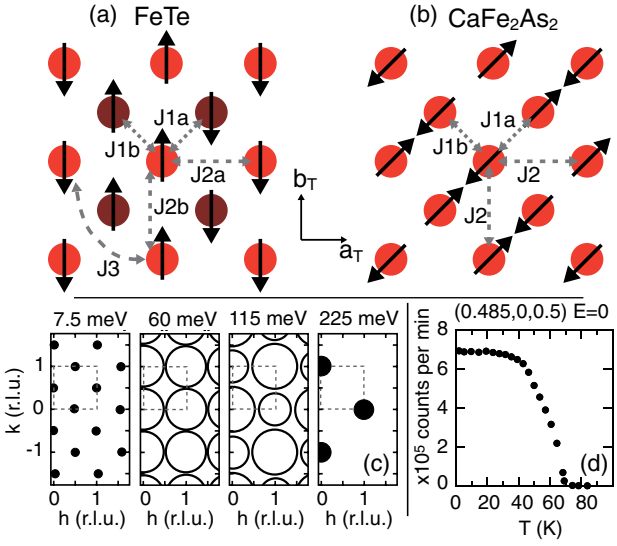

FIG. 1 (color online). (a) Schematic of in-plane Fe spins displaying magnetic order in $Fe_{1+y}Te$ with small y [14,15], and showing definition used for exchange energies. (b) Schematic of in-plane magnetic order in $CaFe_2As_2$ [33] with exchange energy definitions. (c) Schematic showing wave vector dependence of intensity at various energies (for raw data see Fig. 2). Dashed line shows one BZ. (d) Temperature dependence of elastic scattering at magnetic Bragg peak for the $Fe_{1.05}Te$ sample.

member of the isovalently substituted $Fe_{1+y}Te_{1-x}Se_x$ iron chalcogenide superconductors [22,23]. By measuring spin-wave excitations in $Fe_{1.05}Te$ throughout the Brillouin zone (BZ), we have used a Heisenberg Hamiltonian to determine the effective exchange couplings of the system. Our neutron scattering experiments were carried out on the HB-1 triple-axis spectrometer at High Flux Isotope Reactor and on the ARCS chopper spectrometer at Spallation Neutron Source, Oak Ridge National Laboratory, U.S. We also used MAPS chopper spectrometer at ISIS, Rutherford-Appleton Laboratory, UK. For the experiment, we have coaligned 6 g of single crystals of $Fe_{1.05}Te$. All data were collected at around 10 K ($\ll T_N$) with incident neutron energies $E_i =$ 55, 90, 180, 350, 500, and 580 meV with the c axis aligned along the incident beam direction. Since the spin-wave excitations have weak c-axis coupling, we integrate the excitations along the c-axis direction and focus on spin waves in the (h, k) plane.

For $Fe_{1+y}Te$ with modest excess iron content y, the magnetic structure is shown in Fig. 1(a) [14,15], which can be viewed as two AFM sublattices as shown by darker and lighter colored atoms. We define the NN (J_{1a}, J_{1b}), the NNN (J_{2a}, J_{2b}), and the next-next-nearest-neighbor (J_3) exchange interactions as shown in Fig. 1(a) [20]. The NN magnetic exchange couplings (J_{1a}, J_{1b}) are defined similarly to those of iron pnictides [Fig. 1(b)]. However, the NNN couplings (J_{2a}, J_{2b}) in chalcogenides are directionally dependent as shown in Fig. 1(a).

Our $Fe_{1.05}Te$ samples were grown using Bridgman technique as described before [21]. $Fe_{1+y}Te_{1-x}Se_x$ is tetragonal at high temperature and becomes orthorhombic or monoclinic (depending on x, [14,15,22,23]) below T_N. The ab-plane lattice parameters for the various phases remain very similar, and on cooling into the low symmetry phase the sample becomes twinned. We therefore measure the wave vector in tetragonal (h, k, l) reciprocal lattice units, with in-plane lattice parameters $a = b = 3.80$ Å, and the out-of-plane $c = 6.23$ Å. In this notation, magnetic order in powder $Fe_{1+y}Te$ has been found at $(0.5, 0, 0.5)$ for small y, and increasing y will lead to incommensurate magnetic order [14,15]. In the present single crystalline samples, the magnetic order was found to be centered very close to the commensurate position at $(0.485, 0, 0.5)$ r.l.u. and $y = 0.05$ was measured with inductively coupled plasma analysis [21]. However, we also observed a weaker magnetic peak at $(0.37, 0, 0.5)$ r.l.u. attributed to a small portion of the sample with slightly different y. Figure 1(d) shows the temperature dependence of the magnetic Bragg intensity at $\mathbf{Q} = (0.485, 0, 0.5)$ r.l.u. confirming $T_N = 68$ K.

The magnetic excitations probed by neutron scattering in our $Fe_{1.05}Te$ sample are summarized by representative constant energy slices in Fig. 2. The data have been normalized to a vanadium standard and plotted in absolute units, without correction for the magnetic form factor, causing the signal intensity to decrease with increased Q.

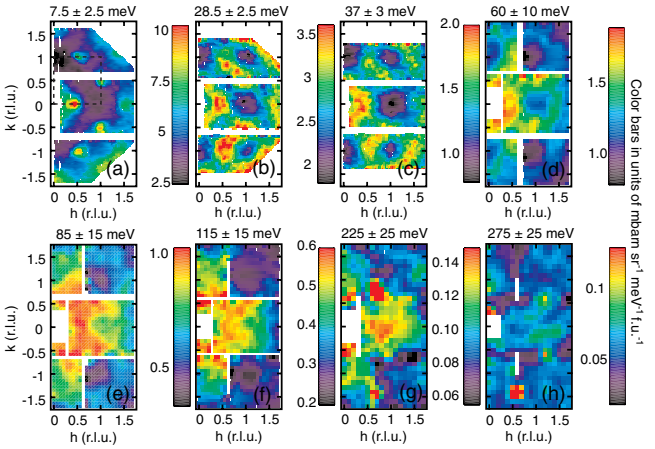

FIG. 2 (color online). Constant energy slices of the spin waves as a function of increasing energy at 10 K for $Fe_{1.05}Te$. All data are normalized to absolute units with a vanadium standard. (a)–(c) Collected with incident neutron energy $E_i = 90$ meV on ARCS, (d)–(f) $E_i = 350$ meV on MAPS, (g),(h) $E_i =$ 500 meV on MAPS. The dashed line in (a) shows a crystallographic BZ.

Each E_i probes a different out-of-plane wave vector for each energy transfer, and it was found that data from different E_i's were consistent, implying little L dependence of the data over the energy range probed.

Spin waves in most materials tend to display a magnetic response centered on the magnetic Bragg position up to the highest energies, with successively larger rings with increased energy. However, we discuss below how the center of the excitations switch from the $(0.5, 0)$ low energy position to integer positions at higher energy, which we interpret as the outcome of the interaction of competing ferromagnetic and AFM exchange energies.

At our lowest energy, 7.5 meV [Fig. 2(a)], magnetic excitations emerge from the AFM Bragg position $(0.5, 0)$ and other half-integer reciprocal lattice vectors [in an untwinned sample, magnetic peaks would not appear at $(0, 0.5)$, but twinning leads to an equal intensity domain rotated by 90° in plane]. As the energy is increased, the response spreads out in Q as expected for spin waves [Figs. 2(b) and 2(c)]. As the energy is raised to around 60 meV [Fig. 2(d)], there are no longer peaks at half-integer positions, but instead there are rings of radii ~0.5 r.l.u. which are centered on integer reciprocal lattice points. These rings are even clearer when the data are corrected for the magnetic form factor dropoff at high wave vector (see supplementary material [24]). As energy is increased, the radii of rings around $(1, 1)$ expand and those around $(1, 0)$ contract [Figs. 2(e) and 2(f)]. Even at 115 meV a ring can be seen around $(1, 0)$, which by 225 meV contracts into a peak at $(1, 0)$ [Fig. 2(g)] before the disappearance of all intensity at higher energies [Fig. 2(h)]. Corresponding cuts along the $(h, 0)$ trajectory are shown in Fig. 3. A schematic of the dispersion of

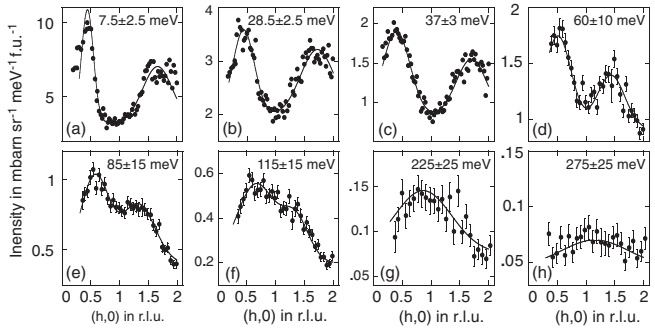

FIG. 3. Constant energy cuts along the $(h, 0)$ trajectory, each from a slice in Fig. 2. Solid lines are fits to Gaussians.

the magnetic response is shown in Fig. 1(c). The data above 100 meV in $Fe_{1.05}Te$ have similarities to the highest energy spin excitations observed in $FeTe_{1-x}Se_x$ with $x = 0.27, 0.49$ [25].

In order to extract effective exchange energies, we fit spin-wave data using a Heisenberg Hamiltonian (see supplementary material [24] for the model Hamiltonian) with commensurate $(0.5, 0, 0.5)$ AFM [26]. In order to yield this commensurate AFM, there are constraints on the bounds of each of the magnetic exchange energies [26]. Because of the twinned nature of the sample, the model used is the sum of two equal sized domains rotated by 90°.

To determine the dispersion curves for spin waves, the slices in Fig. 2 were cut along the $(h, 0)$ and $(1, k)$ directions. By fitting Gaussians to many $(h, 0)$ cuts of different energies like those in Fig. 3, we obtain the dispersion plot in Fig. 4(a) using the fitted peak positions. Similarly, $(1, k)$ cuts were fitted to create Fig. 4(b). These two dispersion plots were simultaneously fitted to the dispersion of the model [26], yielding the fit displayed in Figs. 4(a) and 4(b). Similar conclusions about the dispersion could be reached by viewing the data in terms of constant-Q cuts instead of cuts at constant energy, but this was not found to be as effective for quantitative analysis (see supplementary material [24]). In Fig. 4, the intensity of the excitations of the model is proportional to the radius of the marker (which is saturated at the lowest energies to maintain figure clarity), to highlight the bands with negligible intensity (also see the supplementary material [24] for a zoom into the low energy part of the plots). The presence of almost nondispersive bands around 250 meV is not clear in the Q cuts, possibly because of averaging out in Q as the bandwidth is comparable to the instrument resolution (along with poorer statistics at high energies). It is also not clear if these bands can be seen in constant-Q analysis (see supplementary material [24]).

In the fit lines displayed in Figs. 4(a) and 4(b), J_{2b} was fixed equal to J_{2a}, after it was found that these two parameters had very similar values when allowed to vary (see supplementary material [24] for fit with J_{2b} not fixed to J_{2a}). This four parameter fit leads to exchange energies of $J_{1a} = -17.5 \pm 5.7$, $J_{1b} = -51.0 \pm 3.4$, $J_2 = J_{2a} = J_{2b} = 21.7 \pm 3.5$, $J_3 = 6.8 \pm 2.8$ meV (assuming $S = 1$)

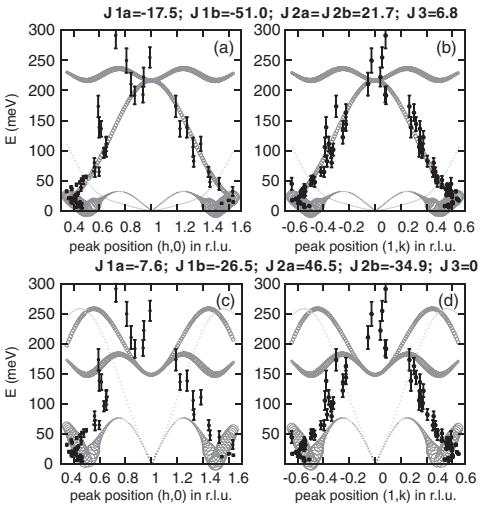

FIG. 4. (a),(b) Solid black markers are dispersion data found from fitting Gaussians to form factor corrected data at many energies for the $(h, 0)$ and $(1, k)$ directions, respectively. Gray open circles (with radius indicating intensity) show best fit dispersion curves with fitting parameters given in the main text. (c),(d) Data as in (a),(b), but with dispersion curves simulated using exchange constants predicted by density functional calculations, which clearly do not agree with the data.

and fits the dispersion in these directions well. By further fixing $J_3 = 0$, the model can successfully fit the data up to ~100 meV, but the maximum band energy $\omega_{\max}$ is underestimated by around 50 meV (see supplementary material [24] for fits where J_3 is fixed to zero).

Using the fit parameters listed above, we show in Fig. 5 constant energy slices calculated from the resolution-convolved model. Here we have also considered the out-of-plane (c-axis) exchange coupling J_z and found that $J_z = 1$ meV best fits the spin-wave intensities, although the simulation slices otherwise do not change significantly with J_z. The overall features of the model fit are (i) below ~30 meV, intensity is located around $(0.5, 0)$, (ii) at intermediate energy there are rings around $(1, 1)$ that grow with increasing energy, and (iii) above ~150 meV the intensity ends in a peak at $(1, 0)$. The data are consistent with the model, though the intermediate energy features are more gridlike than the more rounded data.

Our fits and simulations show highly anisotropic in-plane NN exchange couplings with $|J_{1b}| \gg |J_{1a}|$ and a NNN exchange that is AFM (energy ~20 meV) and isotropic $J_2 = J_{2a} \approx J_{2b}$. The $\omega_{\max}$ observed is between 200–250 meV. Comparing our results to similar high energy measurements of $CaFe_2As_2$ [27], which has $J_{1a} = 50 \pm 10$, $J_{1b} = -5.7 \pm 5$, $J_2 = 19 \pm 3$ meV, and $\omega_{\max} \approx 200$ meV, it is clear that the $\omega_{\max}$ and values of J_2 are similar, as well as the presence of anisotropy in J_1 in both cases plus no anisotropy in J_2 in either case. However, the dominating J_1 exchange constants are -50 meV (J_{1b}) and $+50$ meV (J_{1a}) for $Fe_{1.05}Te$ and $CaFe_2As_2$, respectively.

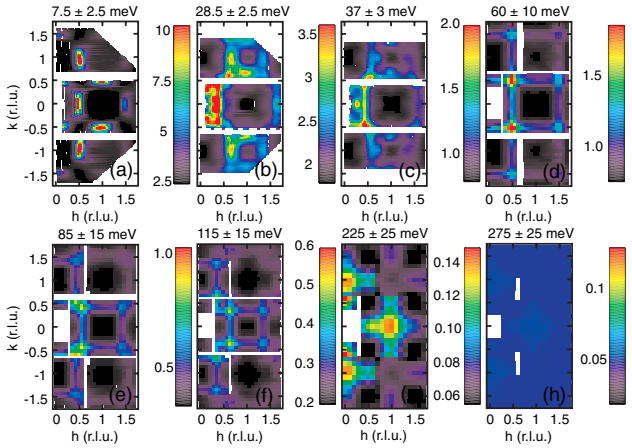

FIG. 5 (color online). Resolution convolved simulation (using TOBYFIT [34]) of the Heisenberg model using the best fit parameters in the text plus an out-of-plane coupling of $J_z = 1$ meV. Each slice corresponds to a slice in Fig. 2. The model has been given a linewidth of 10 meV before resolution convolution, though adjusting the linewidth does not make a substantial difference. All slices are on the same intensity color scale as Fig. 2, with an overall intensity scale that was chosen so that intermediate simulation slices had a similar intensity to the intermediate raw data slices.

Our results shed new light on the nature of the magnetic state in the iron chalcogenides and its relationship to superconductivity. The isotropic J_2 suggests that this NNN exchange coupling originates from the superexchange mechanism and is insensitive to the lattice distortion and variation in the d-orbital components. Theoretically, it has been shown that the NNN [18] magnetic coupling can cause an $s^{\pm}$-wave pairing that induces a neutron spin resonance at wave vector $(0.5, 0.5)$ [28,29]. Similar isotropic AFM J_2 values in iron pnictides and iron chalcogenides therefore naturally explain the experimentally observed neutron spin resonance within both classes of iron-based superconductors [6–12]. First principles density functional calculations [20] on $Fe_{1.068}Te$ predict highly anisotropic NNN exchange interactions which are not consistent with our data [see Figs. 4(c) and 4(d) for dispersion and the supplementary material [24] for simulation slices], perhaps due to the complex nature of the orbital ordering [30,31] or itinerant magnetism [32] in this material.

In summary, we have shown that spin-wave excitations in the iron chalcogenide $Fe_{1.05}Te$ can be modeled by a Heisenberg Hamiltonian with anisotropic (dominantly) ferromagnetic NN and isotropic AFM NNN exchange couplings. While the NN couplings for $Fe_{1.05}Te$ and $CaFe_2As_2$ [27] are different, we find that the AFM NNN exchange couplings in these two classes of materials are not only similar in magnitude but also directionally independent, even though they have different AFM and crystal structures [14,15,33]. Our findings suggest that superconductivity in both classes of iron-based superconductors shares a common magnetic origin that is intimately associated with the AFM NNN exchange couplings [18].

This work is supported in part by the U.S. DOE, BES, through DOE DE-FG02-05ER46202 and by the U.S. DOE, Division of Scientific User Facilities. The work at the IOP is supported by the CAS. O. J. L. and T. E. were supported by the DOE, BES, EPSCoR Grant No. DE-FG02-08ER46528.

*daip@ornl.gov

[1] R. Coldea *et al.*, Phys. Rev. Lett. **86**, 5377 (2001).
[2] P. A. Lee, N. Nagaosa, and X. G. Wen, Rev. Mod. Phys. **78**, 17 (2006).
[3] Y. Kamihara *et al.*, J. Am. Chem. Soc. **130**, 3296 (2008).
[4] D. Johnston, Adv. Phys. **59**, 803 (2010).
[5] A. Subedi *et al.*, Phys. Rev. B **78**, 134514 (2008).
[6] A. D. Christianson *et al.*, Nature (London) **456**, 930 (2008).
[7] M. D. Lumsden *et al.*, Phys. Rev. Lett. **102**, 107005 (2009).
[8] S. Chi *et al.*, Phys. Rev. Lett. **102**, 107006 (2009).
[9] D. S. Inosov *et al.*, Nature Phys. **6**, 178 (2009).
[10] H. A. Mook *et al.*, Phys. Rev. Lett. **104**, 187002 (2010).
[11] Y. Qiu *et al.*, Phys. Rev. Lett. **103**, 067008 (2009).
[12] T. J. Liu *et al.*, Nature Mater. **9**, 718 (2010).
[13] M. J. Han *et al.*, Phys. Rev. Lett. **102**, 107003 (2009).
[14] W. Bao *et al.*, Phys. Rev. Lett. **102**, 247001 (2009).
[15] S. Li *et al.*, Phys. Rev. B **79**, 054503 (2009).
[16] I. I. Mazin and J. Schmalian, Physica (Amsterdam) **469C**, 614 (2009).
[17] K. Kuroki *et al.*, Phys. Rev. Lett. **101**, 087004 (2008).
[18] K. J. Seo, B. A. Bernevig, and J. P. Hu, Phys. Rev. Lett. **101**, 206404 (2008).
[19] F. Wang *et al.*, Phys. Rev. Lett. **102**, 047005 (2009).
[20] M. J. Han and S. Y. Savrasov, Phys. Rev. Lett. **103**, 067001 (2009).
[21] G. F. Chen *et al.*, Phys. Rev. B **79**, 140509(R) (2009).
[22] F. C. Hsu *et al.*, Proc. Natl. Acad. Sci. U.S.A. **105**, 14 262 (2008).
[23] M. H. Fang *et al.*, Phys. Rev. B **78**, 224503 (2008).
[24] See supplemental material at http://link.aps.org/supplemental/10.1103/PhysRevLett.106.057004 for details of the analysis.
[25] M. D. Lumsden *et al.*, Nature Phys. **6**, 182 (2010).
[26] C. Fang, B. A. Bernevig, and J. P. Hu, Europhys. Lett. **86**, 67 005 (2009).
[27] J. Zhao *et al.*, Nature Phys. **5**, 555 (2009).
[28] M. M. Korshunov and I. Eremin, Phys. Rev. B **78**, 140509 (R) (2008).
[29] T. A. Maier *et al.*, Phys. Rev. B **79**, 134520 (2009).
[30] W. C. Lv, F. Krüger, and P. Phillips, Phys. Rev. B **82**, 045125 (2010).
[31] F. Krüger *et al.*, Phys. Rev. B **79**, 054504 (2009).
[32] C. Y. Moon and H. J. Choi, Phys. Rev. Lett. **104**, 057003 (2010).
[33] A. I. Goldman *et al.*, Phys. Rev. B **78**, 100506(R) (2008).
[34] http://tobyfit.isis.rl.ac.uk